CHAPTER 2

Voltage Gated Ionic Currents

Christopher P. Fall and Joel E. Keizer

In Chapter 1 we introduced models of simple channel behavior but ignored the idea that something might flow through such a channel. In this chapter we will learn how to model current flowing through ion channels and how to include the feedback regulation of the channel behavior by voltage. But let us be very clear about what we are modeling in this chapter. Only in the most idealized sense are we modeling the behavior of excitable cells like neurons. In fact, we will be creating *point models* of patches of membrane, with only implicit consideration through the use of ion concentrations of the idea that the membrane encloses a compartment. We do not consider at all that a neuron is a highly complicated cell that integrates signals within *dendrites* and a *soma* before producing *action potentials* in an excitable *axon*. Some of the diverse neuronal shapes are shown in Figure 2.1.

Electrophysiology is the study of ionic currents and electrical activity in cells and tissues. Because this field has its roots in classical physics, traditionally it has been the most quantitative field in cell physiology. The groundbreaking work of the physiologists Hodgkin and Huxley and others in elucidating the mechanism of action potentials in the squid giant axon before and after the Second World War was the first major breakthrough of dynamical modeling in physiology. In the latter half of the twentieth century, the introduction of the patch-clamp technique established firmly that ionic currents are carried by proteins that act as gated ionic pores. More recently, genetic engineering techniques have been employed to clone, modify, and characterize the gating mechanisms of many types of channels (Hille 2001).

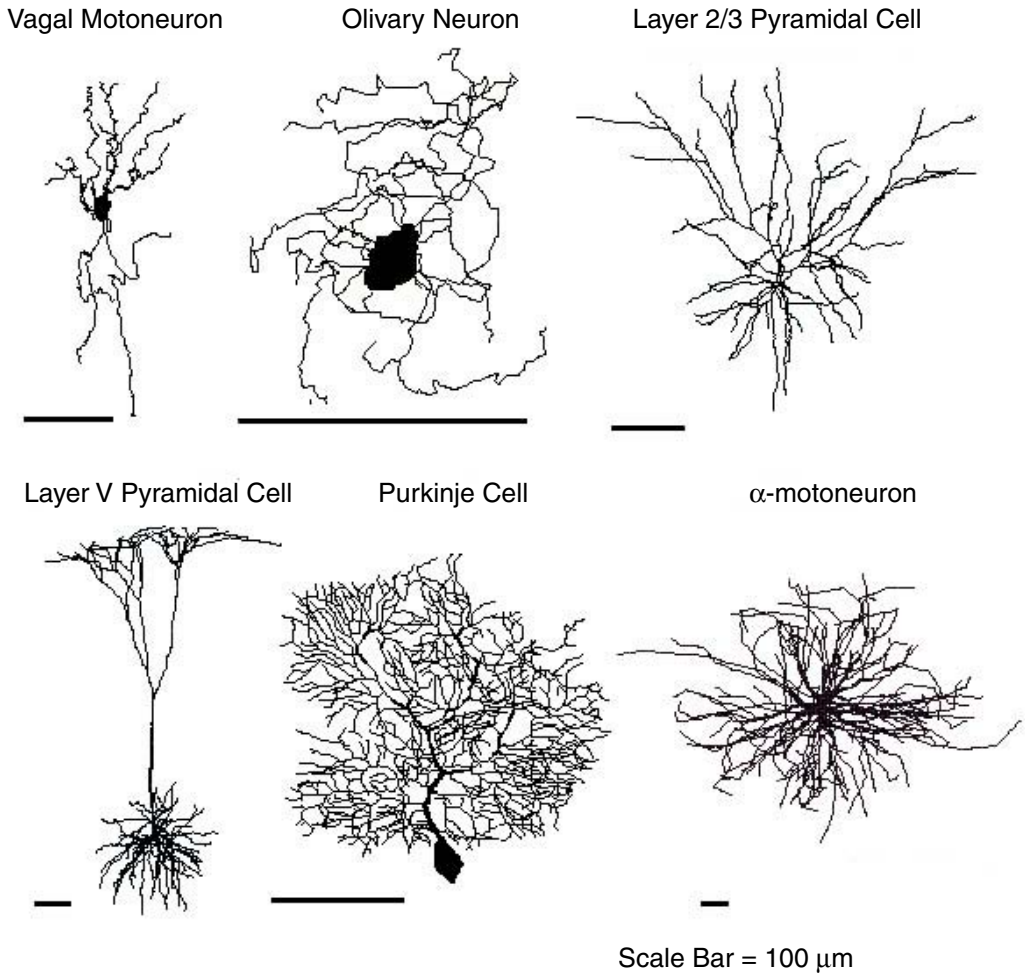

Figure 2.1 Examples of the diverse shapes of mammalian neurons. Reprinted from Koch and Segev (2000).

In this chapter we focus on voltage gated ionic currents. We begin by reviewing the basic concepts of electrical behavior in cells. Next, we describe classical activation and inactivation kinetics and how the voltage clamp technique can be used to study these currents. We use the Morris–Lecar model for action potentials in the giant barnacle muscle to illustrate how voltage gated channels can interact to produce oscillations and action potentials. The Morris–Lecar model is nonlinear but involves only two variables. With only two variables, we can analyze the dynamics of the equations for this model using phase plane techniques. For completeness, we close with brief introductions to the Hodgkin–Huxley model of the squid giant axon and FitzHugh–Nagumo models.

Table 2.1 Important Definitions in Electrophysiology

Definition	Abbreviation	Value
Avogadro's number	N	$6.02 \cdot 10^{23}$ /mol
Faraday's constant	F	$9.648 \cdot 10^{4}$ C/mol
elementary charge	e	$1.602 \cdot 10^{-19}$ C
gas constant	R	8.315 J/(mol · K)
joule	J	1 V · C
volt	V	1 J/C
ampere	A	1 C/s

2.1 Basis of the Ionic Battery

The electrical behavior of cells is based upon the transfer and storage of charge. We are used to thinking about electricity as the movement of electrons, but current can be carried by any charged particle, including ions such as K^+, Na^+, and Ca^{2+} in solution. As we will see, the ability of cells to generate electrical signals is entirely dependent on the evolution of ion–specific pumps and pores that allow the transfer of charge up and down gradients. Ion pumps use energy in the form of ATP to transport ions against a concentration gradient.

Before we begin our discussion of the ionic battery, it is usefull to recall several important definitions from elementary physics listed in Table 2.1. An ion's *valence* is the number of charges, plus or minus, that it carries. A given number of *divalent* Ca^{2+} ions would carry twice the amount of charge as the same number of *univalent* K^+ ions.

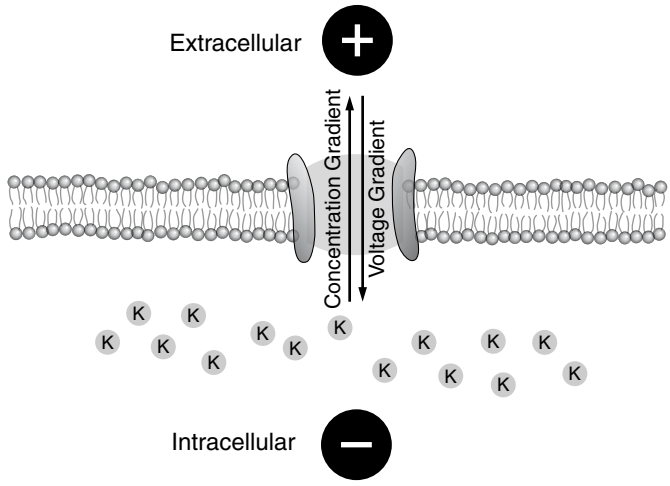

Figure 2.2 The basis of the ionic battery. Adapted from McCormick (1999).

Using these relationships, we see that the transfer of 1 mole of K^+ ions in a period of one second would carry a current equal to Faraday's constant. It requires one joule of energy (i.e. ATP consumed by ion pumps) to separate one coulomb of charge across one volt of potential (which is the definition of volt).

2.1.1 The Nernst Potential: Charge Balances Concentration

Biological fluids such as cytoplasm and extracellular fluid contain numerous ions. Consider the case where the two ions K^+ and any monovalent anion A^- are in solution such that the concentration is different across the impermeable membrane but the two ions are equal in concentration on the same side of the membrane. As shown in Figure 2.3A, before we make any changes, there is no potential difference across the membrane because the charge between the K^+ ions and the A^- ions is balanced on each side due to the equivalent concentrations. As shown in Figure 2.3B, if we insert a nonselective pore into the membrane, concentration and charge equilibrate such that there are equal concentrations of each ion on both sides of the membrane, and the voltage across the membrane is again zero.

It is when we insert into the membrane an ion-selective pore that allows only the passage of K^+ that the phenomenon shown in Figure 2.3C occurs. Because $[K^+]$ is greater on one side of the membrane, K^+ ions diffuse through the K^+ pore down the concentration gradient. Because the membrane is not permeable to the anion A^-, each K^+ ion that passes down the concentration gradient carries a positive charge that is not balanced by an accompanying A^-. Because the transfer of these charges establishes

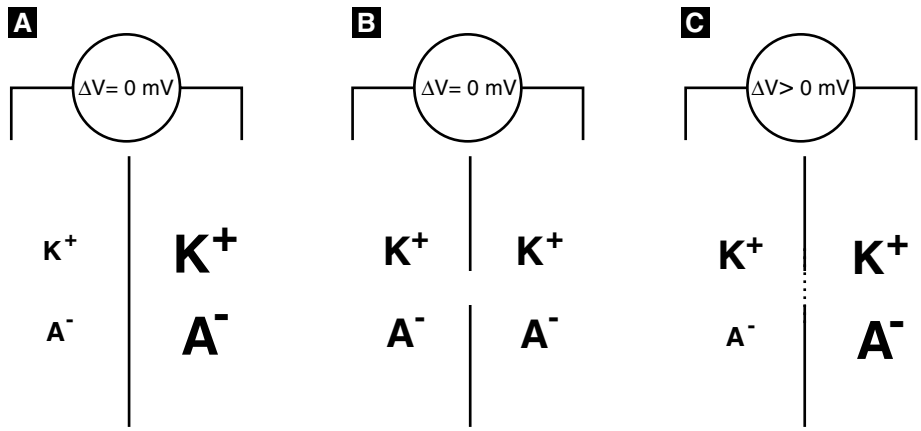

Figure 2.3 (A) Concentration and charge are balanced on each side of the membrane, so there is no ΔV across the membrane. (B) Due to the nonselective pore, charge and concentration are balanced everywhere, and so there is no ΔV across the membrane. (C) A K^+ selective pore allows K^+ but not A^- to pass through the membrane. K^+moves to equilibrate concentration until counterbalanced by the accumulating negative charge, because A^- cannot move. The "voltmeter" is seeing excess + charge on the left side and excess − charge on the right side.

an electrical potential gradient, K^+ ions continue to move from high concentration to low concentration until the growing force due to the electrical potential difference is balanced by the (opposite) force generated by the concentration difference.

The *equilibrium potential*, where the electrical and osmotic forces are balanced, is given by the *Nernst equation*. The Nernst equation is derived from the expression for the change in Gibbs free energy when one mole of an ion of valence z is moved across a membrane:

$$\Delta G = -RT \ln \frac{[\text{ion}]_{\text{out}}}{[\text{ion}]_{\text{in}}} + \Delta VFz. \tag{2.1}$$

At equilibrium, ΔG is zero. Rearranging gives us the Nernst potential:

$$\begin{aligned} \Delta V = V_{\text{Nernst}} &= \frac{RT}{zF} \ln \frac{[\text{ion}]_{\text{out}}}{[\text{ion}]_{\text{in}}} \\ &= 2.303 \frac{RT}{zF} \log_{10} \frac{[\text{ion}]_{\text{out}}}{[\text{ion}]_{\text{in}}} \\ &= \frac{61.5}{z} \log_{10} \frac{[\text{ion}]_{\text{out}}}{[\text{ion}]_{\text{in}}} \text{ (at } 37^\circ\text{C)} \end{aligned} \tag{2.2}$$

where R and F are given in Table 2.1, T is temperature (in kelvin), and z is the valence of the ion as previously defined. At body temperature, RT/F is approximately 60 mV. Therefore, a 10–fold difference in the concentration of a monovalent ion like K^+ would result in approximately -60 mV of potential difference across a membrane ($[K^+]$ is greater inside a neuron). Because the Nernst potential represents the equilibrium of the thermodynamic system, the potential difference evolves to that given by the Nernst equation regardless of the initial starting potential. This tendency for the system to move toward the equilibrium potential is the basis of the *ionic battery* used in the modeling of electrophysiological phenomena. In electrophysiology, the equilibrium potential is called the *reversal potential*, because departure from that point of zero current flux results in the positive or negative flow of ions .

Table 2.2 Resting Ion Concentrations. From McCormick (1999).

Ion	Cytoplasmic Concentration (mM)	Extracellular Concentration (mM)
Squid Giant Axon		
K^+	400	20
Na^+	50	440
Cl^-	40	560
Mammalian Neuron		
K^+	135	3
Na^+	18	145
Cl^-	7	120

2.1.2 The Resting Membrane Potential

The Nernst potential is the equilibrium potential for one permeant ion. In reality, no channel is perfectly selective for a given ion, and there are various channels selective for various ions in a given cell as well. The Goldman–Hodgkin–Katz (GHK) equation is related to the Nernst equation, but considers the case where there are multiple conductances. The GHK equation determines the resting membrane potential of a cell from a weighted sum of the various conductances:

$$V_{\mathrm{GHK}} = \frac{RT}{F} \ln \frac{P_{\mathrm{K}}[\mathrm{K}^+]_{\mathrm{out}} + P_{\mathrm{Na}}[\mathrm{Na}^+]_{\mathrm{out}} + P_{\mathrm{Cl}}[\mathrm{Cl}^-]_{\mathrm{in}}}{P_{\mathrm{K}}[\mathrm{K}^+]_{\mathrm{in}} + P_{\mathrm{Na}}[\mathrm{Na}^+]_{\mathrm{in}} + P_{\mathrm{Cl}}[\mathrm{Cl}^-]_{\mathrm{out}}} \tag{2.3}$$

where P_i is the relative permeability for ion i, which must be determined experimentally. While it looks like a straightforward extension of the Nernst equation, the GHK equation requires assumptions about both the interaction of ions and their ability to diffuse within channels.

We are not going to deal with these complicating details here, and in addition, we will assume perfect selectivity for our ion channels. If we define the *conductance*, $g = 1/R$ as the reciprocal of the resistance, we can use a similar weighted–sum formalism for calculating the membrane potential of a cell:

$$V_{\mathrm{m}} = \frac{\sum_i (V_i \cdot g_i)}{\sum_i g_i}, \tag{2.4}$$

where V_i is the Nernst–equation–derived reversal potential for ion i calculated using (2.2). For example, the membrane potential for a cell containing Na^+, K^+, and Cl^- ions would be

$$V_{\mathrm{m}} = \frac{(V_{\mathrm{Na}} \cdot g_{\mathrm{Na}}) + (V_{\mathrm{K}} \cdot g_{\mathrm{K}}) + (V_{\mathrm{Cl}} \cdot g_{\mathrm{Cl}})}{g_{\mathrm{Na}} + g_{\mathrm{K}} + g_{\mathrm{Cl}}}. \tag{2.5}$$

This is the expression for the resting membrane potential that we will use throughout the remainder of the book. Because the resting membrane potential is the weighted average of Nernst potentials for the various ions, the ion with the greatest permeability contributes the most (see Exercise 1c).

The Nernst potential represents an equilibrium between electrical and osmotic forces on an ion across a membrane: It is what the membrane potential would be if a particular ion were at equilibrium across a membrane. Each ion has its own characteristic Nernst potential given by equation (2.2), which is determined by its concentration gradient across the membrane. The actual membrane potential is some "average" of the Nernst potentials of the several ions that are able to cross the membrane; each ion contributing to the actual membrane potential according to the permeability (or conductance) of the membrane for that particular ion. The resting potential across a membrane given by (2.5) is a steady state in which the currents carried by different ions across the membrane cancel each other out. The GHK potential is a steady state solution of a different kinetic equation for total current, based on different assumptions about how ions cross the membrane.

2.2 The Membrane Model

We know from Ohm's law that current flows down a voltage gradient in proportion to the resistance in the circuit. Current is therefore expressed as

$$I = \frac{V}{R} = gV. \tag{2.6}$$

To a first approximation, our task in modeling electophysiological phenomena is to describe how the conductance of the membrane to various ions changes with time and then to keep track of the changes in current and voltage that result.

The conceptual idea behind contemporary electrophysiological models originates in the work of K.S. Cole, who pioneered the notion that cell membranes could be likened to an electronic circuit (Cole 1968). Cole's basic circuit elements are (1) the phospholipid bilayer, which acts as a capacitor in that it accumulates ionic charge as the electrical potential across the membrane changes; (2) the ionic permeabilities of the membrane, which act as resistors in an electronic circuit; and (3) the electrochemical driving forces, which act as batteries driving the ionic currents. These ionic and capacitive currents are arranged in a parallel circuit, as shown in Figure 2.4. This analogy to electrical circuits is now widely relied upon for developing models of electrical activity in membranes.

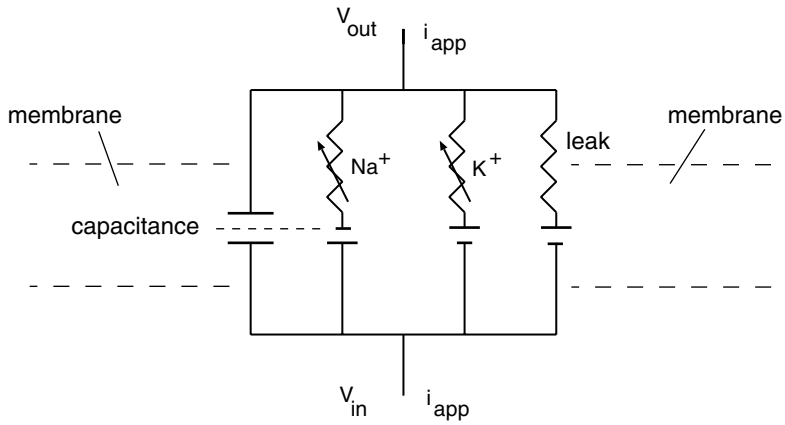

Figure 2.4 The equivalent electrical circuit for an electrically active membrane. The capacitance is due to the phospholipid bilayer separating the ions on the inside and the outside of the cell. The three ionic currents, one for Na^+, one for K^+, and one for a non–specific leak, are indicated by resistances. The conductances of the Na^+ and K^+ currents are voltage dependent, as indicated by the variable resistances. The driving force for the ions is indicated by the symbol for the electromotive force, which is given in the model by the difference between the membrane potential $V = V_{in} - V_{out}$ and the reversal potential.

2.2.1 Equations for Membrane Electrical Behavior

Given the several conductances and their reversal potentials, we calculate using (2.5) what the membrane potential will be after the system has stabilized. This equations for the resting membrane potential tell us nothing about how the system evolves to the steady state. Because we are interested in the time course of the membrane voltage, we have to study the dynamics of the various currents that flow in and out of the cell. We can approximate the current flow through a single K^+ channel using Ohm's law and an assumption that the reversal potential stays constant:

$$I_K = -g_K(V - V_K). \tag{2.7}$$

Here g_K is the conductance of the K^+ channel and the leading negative sign is necessary because of our definitions for "in" and "out." V_K is the K^+ reversal potential determined by the Nernst equation, and $V - V_K$ represents the driving force across the membrane provided by the ionic battery. We assume that the reversal potential for a given ion remains constant, which is equivalent to assuming that restorative mechanisms such as ionic pumps can keep pace with electrical activity on a time scale that prevents the ionic battery from running down. This is a reasonable assumption for a large cell, which would have a small surface area to volume ratio. In a small cell, with a large surface to volume ratio, the ion transfer necessary to change the membrane potential might have a large effect on the intracellular ionic concentration and thus the strength of the ionic battery (see Exercise 2e).

Of course, numerous ions are responsible for the electrical behavior in a cell, and the total current is the sum of the individual ionic currents.

$$I_{ion} = \sum I_i = \sum -g_i(V - V_i) = -g_K(V - V_K) - g_{Na}(V - V_{Na}) - \cdots. \tag{2.8}$$

To translate the electric circuit diagram into ODEs, we use the traditional interpretation of each circuit element along with Kirchoff's law. Assuming that the membrane acts as a capacitor, the capacitive current across the membrane can be written

$$I_{cap} = C\frac{dV}{dt}, \tag{2.9}$$

where C is the capacitance of the membrane and V is the membrane potential, defined as the electrical potential difference between the inside and outside of the cell. To establish the differential equation satisfied by the voltage V, Kirchoff's law of charge conservation is applied to the circuit in Figure 2.4. Kirchoff's law dictates that capacitive current must balance with the ionic current and any currents that might be applied, say, through experimental manipulation. This implies that

$$I_{cap} = I_{ion} + I_{app}, \tag{2.10}$$

where the sum is over all the ionic currents. Using the expressions in (2.8)–(2.10) this can be rewritten

$$C\frac{dV}{dt} = -\sum_i g_i(V - V_i) + I_{app}. \tag{2.11}$$

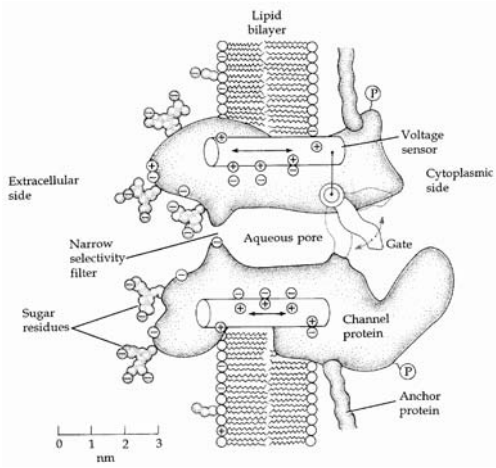

Figure 2.5 Mechanistic cartoon of a gated ionic channel showing an aqueous pore that is selective to particular types of ions. The portion of the transmembrane protein that forms the "gate" is sensitive to membrane potential, allowing the pore to be in an open or closed state. Reprinted from Hille (2001).

To solve this differential equation for voltage, we must know how the gated conductances g_i depend on V (and possibly time). In general, the g_i will not be linear functions of V, and therefore the problem is to find the time and possible voltage dependence of the various conductances.

2.3 Activation and Inactivation Gates

Channels can be thought to have *gates* that regulate the permeability of the pore to ions, as illustrated schematically in Figure 2.5. These gates can be controlled by membrane potential, producing *voltage gated* channels; by chemical ligands, producing *ligand gated* channels; or by a combination of factors. In a series of experiments, Alan Hodkgin, Andrew Huxley, and others established experimentally the voltage dependence of ion conductances in the electrically excitable membrane of the squid giant axon (Hodgkin and Huxley 1939). Hodgkin and Huxley shared a Nobel Prize with John Eccles in 1963 for work on nerve signaling.

2.3.1 Models of Voltage–Dependent Gating

The mathematical description of voltage–dependent activation and inactivation gates is based on the mechanism

$$C \underset{k^-}{\overset{k^+}{\rightleftharpoons}} O, \tag{2.12}$$

which was presented in Chapter 1. What distinguishes a voltage–dependent gating mechanism from a passive mechanism is the voltage dependence of the rate constants.

Recall from (1.1)–(1.5) that the fraction of open channels f_O satisfies the differential equation

$$\frac{df_O}{dt} = \frac{-(f_O - f_\infty)}{\tau}, \tag{2.13}$$

where

$$f_\infty = \frac{k^+}{k^+ + k^-} \text{ and } \tau = \frac{1}{k^+ + k^-}. \tag{2.14}$$

Because ionic channels are composed of proteins with charged amino acid side chains, the potential difference across the membrane can influence the rate at which the transitions from the open to closed state occur. According to the Arrhenius expression for the rate constants, the membrane potential V contributes to the energy barrier for these transitions:

$$k^+ \propto \exp\left(\frac{-\Delta V^+}{RT}\right) \quad \text{and} \quad k^- \propto \exp\left(\frac{-\Delta V^-}{RT}\right). \tag{2.15}$$

The rate constants will have the form

$$k^+ = k_o^+ \exp(-\alpha V) \quad \text{and} \quad k^- = k_o^- \exp(-\beta V), \tag{2.16}$$

where k_o^+ and k_o^- are independent of V. Substituting the relationships in (2.16) into the expressions for f_∞ and τ and rearranging, we obtain

$$f_\infty = \frac{1}{1 + k_o^-/k_o^+ \exp((\alpha - \beta)V)}, \tag{2.17}$$

$$\tau = \frac{1}{k_o^+ \exp(-\alpha V)} \cdot \frac{1}{1 + k_o^-/k_o^+ \exp((\alpha - \beta)V)}. \tag{2.18}$$

We can define

$$S_o = \frac{1}{\beta - \alpha} \tag{2.19}$$

and

$$V_o = \frac{\ln(k_o^-/k_o^+)}{\beta - \alpha}. \tag{2.20}$$

If we substitute S_o and V_o into (2.17) and (2.18) (see Exercise 4), we have

$$f_\infty = \frac{1}{1 + \exp(-(V - V_o)/S_o)} \tag{2.21}$$

$$\tau = \frac{\exp(\alpha V)}{k_o^+} \cdot \frac{1}{1 + \exp(-(V - V_o)/S_o)}. \tag{2.22}$$

Finally, both of these expressions can be rewritten in terms of hyperbolic functions (Exercise 5):

$$f_\infty = 0.5(1 + \tanh((V - V_o)/2S_o)), \tag{2.23}$$

$$\tau = \frac{\exp(V(\alpha + \beta)/2)}{2\sqrt{k_o^+ k_o^-}\cosh((V - V_o)/2S_o)}. \tag{2.24}$$

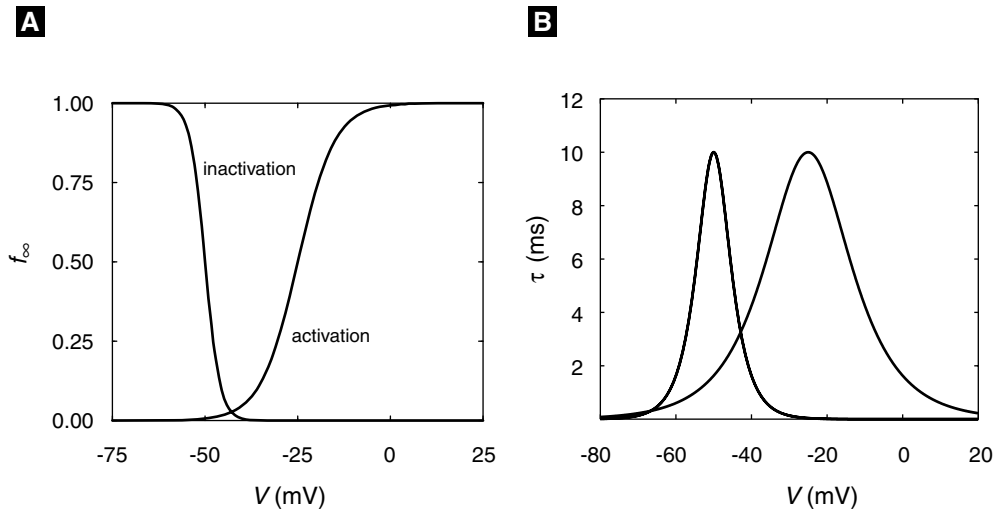

Figure 2.6 (A) Equilibrium open fractions (f_∞) for an inactivation gate ($V_o = -50$ mV and $S_o = -2$ mV) and activation gate ($V_o = -25$ mV and $S_o = 5$ mV) as a function of voltage. (B) The characteristic relaxation times τ for the activation and inactivation gates in (A) as a function of voltage, which are peaked around the values of V_o and have a width determined by S_o.

Recall that f_∞ gives the fraction of channels open at equilibrium at the membrane potential V. Thus for a fixed value of V it gives the open fraction after transient changes in f_O have damped out with a characteristic time τ.

An activation gate tends to open and an inactivation gate tends to close when the membrane is depolarized. Whether a gate activates or inactivates with depolarization is determined by the sign of S_o: a positive sign implies activation and a negative sign inactivation. This is illustrated in Figure 2.6A, where the dependence of f_∞ on V has been plotted for an activation gate with $V_o = -25$ mV and $S_o = 5$ mV and an inactivation gate with $V_o = -50$ mV and $S_o = -2$ mV.

Notice that the magnitude of $S_o$determines the steepness of the dependence of f_∞ on V, whereas the value of $V_o$determines the voltage at which half of the channels are open. The dependence of τ on V for these activation and inactivation gates is illustrated in Figure 2.6B (assuming that $\alpha = -\beta$ and $2\sqrt{k_o^+ k_o^-} = 0.2$ ms^{-1}). When $\alpha = -\beta$ and $\phi = 1/\left(2\sqrt{k_o^+ k_o^-}\right)$,

$$\tau = \frac{\phi}{\cosh((V - V_o)/2S_o)}. \tag{2.25}$$

2.3.2 The Voltage Clamp

In order to measure the voltage across a cell membrane or the current flowing through a membrane, microelectrodes are inserted into cells. These electrodes can be used both

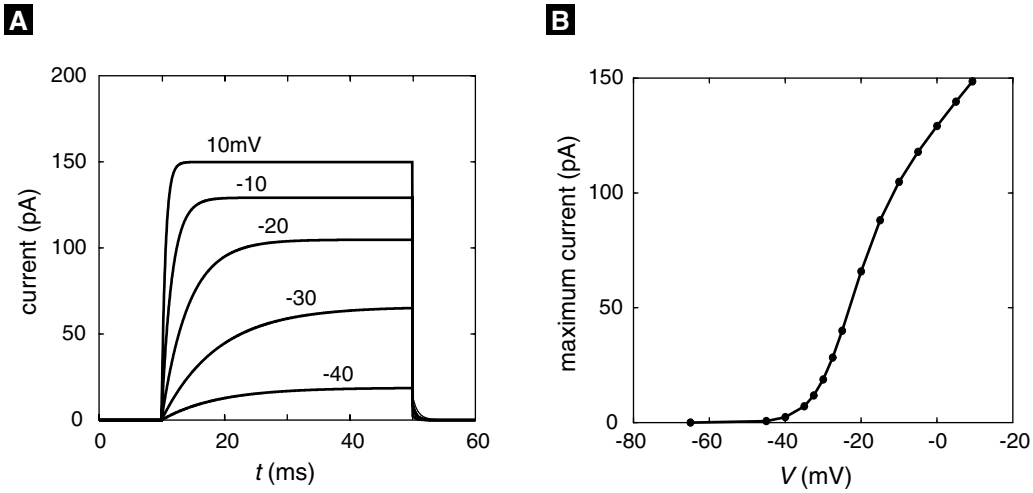

Figure 2.7 Simulation of voltage clamp experiment using (2.28) and (2.29). (A) Current records resulting from 40 ms depolarizations from the holding potential of −60 mV to the indicated test potentials. (B) the maximum (steady state) current as a function of test potential taken from records like those in (A).

to measure current and voltage and to apply external current. In order to measure the voltage dependence of the activation and inactivation of ion conductances, a technique called the *voltage clamp* is used. This is an electronic feedback device that adjusts the applied current I_{app} to match and counter the membrane currents such that the membrane voltage is held constant. To see what this accomplishes, consider a membrane with a single gated ionic current. If we assume that the total conductance is the result of the activation of many channels, the conductance g that we have used above can be defined as the product of the maximum possible conductance $\bar{g}$ and the fraction of open channels f_O that we have already encountered.

$$g = f_O \bar{g}. \tag{2.26}$$

Table 2.3 Consistent Electrical Units

Name (Symbol)	Units	Abbreviation
voltage (V)	10^{-3} volt	mV
time (t)	10^{-3} second	ms
conductance (g)	10^{-9} siemens	nS
capacitance (C)	10^{-12} farad	pF
current (I)	10^{-12} ampere	pA

We can include this new relationship in the differential equation for membrane potential that we have already seen:

$$C\frac{dV}{dt} = -f_O\bar{g}(V - V_{\text{rev}}) + I_{\text{app}}, \tag{2.27}$$

where V_{rev} is the reversal potential given by the Nernst equation. If we can apply a current that is equal and opposite to the current flowing through the membrane,

$$I_{\text{app}} = \bar{g}\xi(V - V_{\text{rev}}), \tag{2.28}$$

then the right–hand side of (2.27) is zero and the voltage must be constant. Because V is constant, $\xi = f_O$ and the time dependence of the applied current comes only from the dependence of f_O on t as determined by the gating equation covered in Chapter 1:

$$\frac{d\xi}{dt} = \frac{-(f_O - f_\infty)}{\tau}. \tag{2.29}$$

Thus the time dependence of the applied current provides a direct measurement of the gated current at a fixed voltage. Note that throughout the remainder of the text we will drop the overbar with the understanding that conductances g_i refer to maximum conductances to be scaled by gating variables.

To carry out a voltage clamp measurement like this it is necessary to block all but a single type of current. While this is not always possible, specific toxins and pharmacological agents have proven useful. For example, tetrodotoxin (TTX) from the puffer fish selectively blocks voltage gated Na^+ currents.

It is not difficult to simulate a voltage clamp measurement using (2.28)–(2.29). However, to carry out either an experimental measurement or a simulation, a consistent set of electrical units must be used. As we have seen, the standard unit for membrane potential is millivolts (mV), and because the characteristic times for voltage–dependent gates τ are in milliseconds (ms), this is taken as the standard unit of time. Currents are typically expressed in μA/cm^2 and capacitances as μF/cm^2. For a typical cell of area 10^{-6} cm^2, this translates to a whole–cell current of picoamperes (1 pA $= 10^{-12}$ A) and a whole cell capacitance of picofarads (1 pF $= 10^{-12}$ F). Cellular dimensions are usually reported in micrometers ("microns"), and there are 10^{-8} square centimeters per square micron. Because most biological channels have a conductance g on the order of 1 to 150 pS, whole–cell conductances of nanosiemens are usually expressed in mS/cm^2, because the units of $V - V_{\text{rev}}$ are mV. This standard set of units is summarized in Table 2.3. An alternative consistent set of units uses current in femtoamperes (1 fA $= 10^{-15}$ A), conductance in pS, and capacitance in fF.

To simulate a voltage clamp experiment we have solved (2.29) and plotted the resulting current given by (2.28). The simulation shown in Figure 2.7A represents a typical set of experiments in which the membrane potential is clamped at a holding potential (-60 mV in Figure 2.7), then changed to various test potentials for a fixed interval (40 ms), and finally returned to the holding potential. The value of the holding potential generally is chosen so that there is little or no current through the channel. This greatly simplifies the interpretation of the current at the test voltages. Figure 2.7A shows the

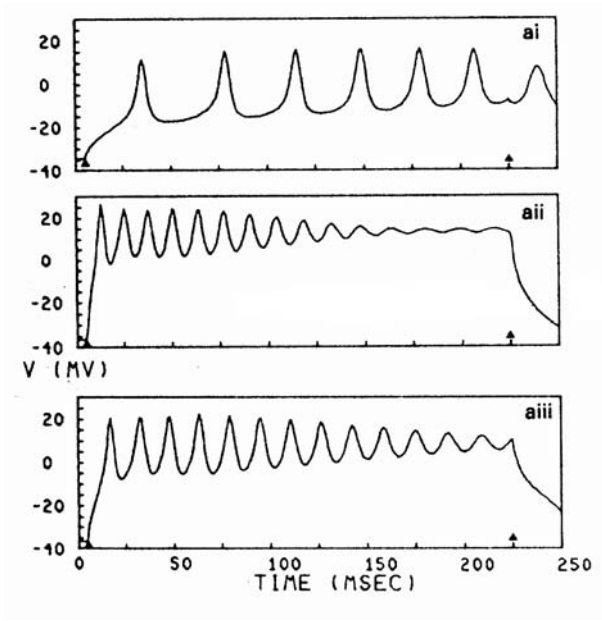

Figure 2.8 Depolarization-induced electrical activity in giant barnacle muscle fibers; the arrows indicated the start and end of the depolarizating currents. Reprinted from Morris and Lecar (1981).

current that develops during this protocol for 5 test voltages V_{test}. The increase in current when the potential is clamped at the test values is governed by the exponential increase in f_O with characteristic time $\tau(V_{\text{test}})$. When the potential is clamped again at the holding potential, the resulting current is called the *tail current*. Its decline is also exponential, but because $V = -60$ mV during this period, the characteristic time is now $\tau(-60\text{ mV})$.

Figure 2.7B gives a plot of the steady–state current as a function of the test voltage. According to (2.28) it can be expressed as $I = gf_\infty(V - V_{\text{rev}})$. Thus for an activating current like that in the simulations, when V is large enough, $f_\infty \approx 1$ and the current is a linear function of V. The curvature in Figure 2.7B at lower voltages is caused by the shape of the activation function f_∞. In the jargon of circuit theory, currents like this are said to *rectify*. The delay in the onset of the maximum current, which is determined by the value of τ, has led to channels like the one simulated in Figure 2.7 being referred to as *delayed rectifiers*.

2.4 Interacting Ion Channels: The Morris–Lecar Model

Application of a depolarizing current to barnacle muscle fibers produces a broad range of electrical activity. Figure 2.8 illustrates the sort of oscillations that are induced by current injections of 180, 540, and 900 μA/cm^{-2} into these fibers. Careful experimental work by a number of research groups has indicated that the giant barnacle muscle fiber contains primarily voltage gated K^+ and Ca^{2+} currents along with a K^+ current

that is activated by intracellular Ca^{2+}, a so-called K^+_{Ca} current. Neither of the voltage gated currents shows significant inactivation in voltage clamp experiments. The trains of depolarization-induced action potentials in Figure 2.8 must occur via a mechanism different from that proposed by Hodgkin and Huxley for the squid giant axon, which, as we will see later, include channel inactivation.

Morris and Lecar proposed a simple model to explain the observed electrical behavior of the barnacle muscle fiber (Morris and Lecar 1981). Their model involves only a fast activating Ca^{2+} current, a delayed rectifier K^+ current, and a passive leak. They tested the model against a number of experimental conditions in which the interior of the fiber was perfused with the Ca^{2+} chelator EGTA in order to reduce activation of the K_{Ca} current. Their simulations provide a good explanation of their experimental measurements. The model translates into two equations:

$$C\frac{dV}{dt} = -g_{Ca}m_\infty(V - V_{Ca}) - g_K w(V - V_K) - g_L(V - V_L) + I_{app}, \tag{2.30}$$

$$\frac{dw}{dt} = \frac{\phi(w_\infty - w)}{\tau}. \tag{2.31}$$

Here m_∞ is the fraction of voltage-dependent Ca^{2+}channels open, and this is a function of voltage but not time. Furthermore, w is the fraction of open channels for the delayed rectifier K^+ channels, and the conductances g_L, g_{Ca}, and g_K are for the leak, Ca^{2+}, and K^+ currents, respectively. We use w rather than the previously used f_O for the fraction of open channels for historical reasons. The functions

$$m_\infty = 0.5[1 + \tanh((V - v_1)/v_2)], \tag{2.32}$$

$$w_\infty = 0.5[1 + \tanh((V - v_3)/v_4)], \tag{2.33}$$

$$\tau = 1/\cosh((V - v_3)/(2 \cdot v_4)), \tag{2.34}$$

Table 2.4 Morris–Lecar Oscillator Parameters (Type II)

Parameter	Value
C	$20\mu F/cm^2$
V_K	-84 mV
g_K	8 mS/cm^2
V_{Ca}	120 mV
g_{Ca}	4.4 mS/cm^2
V_{leak}	-60 mV
g_{leak}	2 mS/cm^2
$v1$	-1.2 mV
$v2$	18 mV
$v3$	2 mV
$v4$	30 mV
ϕ	0.04/ms

are the equilibrium open fractions for the Ca^{2+} current and the K^+ current, and the activation time constant for the delayed rectifier. Representative parameters are given in Table 2.4. Again note that m is not a dynamic variable. The reason for this is that we have assumed that the time constant for m is short enough that m is always in steady state, $m = m_\infty$. The idea of fast and slow processes is arguably one of the most important concepts in modeling. Although we make the assumption without argument here, its implications in modeling are addressed in a more mathematical context in Chapter 4 and Appendix A.

We have solved the Morris–Lecar equations for four values of the applied current I_{app} and plotted the time series for V in Figure 2.9A. Current in the Morris–Lecar model is specified in μA/cm^2, however to simplify notation somewhat we will assume that the cell has a total surface area of 10^{-6} cm^2, so that μA/cm^2 corresponds to 1 pA of total current. In the absence of applied current the equations have a stable steady state near -60 mV. Although increasing I_{app} to 60 pA produces a brief transient action potential, the effect of the depolarization simply produces a steady state near -35 mV. Depolarization with a current of 150 pA, on the other hand, produces a steady train of action potentials reminiscent of those observed experimentally in Figure 2.8. In the presence of depolarizing currents much greater than this, the simulated barnacle cell can no longer sustain continuous spiking, as shown at $I_{\text{app}} = 300$pA.

2.4.1 Phase Plane Analysis

The mechanistic features underlying continuous spiking and action potentials can be understood easily using phase plane analysis. Because of the ease of representation in two dimensions, two variable models such as the Morris–Lecar model are particularly amenable to this technique. Phase plane analysis is a powerful way to determine how the behavior of a system will change with changes in the various parameters in a system. Several types of plots are utilized as part of what is generically called phase plane analysis:

- a *phase portrait* consists of the variables describing a system plotted against each other rather than as a function of time to produce a *trajectory* in *phase space*. A phase portrait tells us how the variables interact for a given set of parameters.
- A *vector field* shows us the direction in which a system will evolve from any location in phase space.
- *Nullclines* are plotted in phase space, and show us the values of a pair of variables at which one of the variables does not change. In other words, for a coupled system of equations $X(x, y, t)$ and $Y(x, y, t)$ nullclines are the solutions to the equations

$$\frac{dX}{dt} = 0, \ \frac{dY}{dt} = 0 \tag{2.35}$$

Note that there is a nullcline for each variable. The points of intersection of two nullclines are particularly interesting points in phase space that we will discuss below.

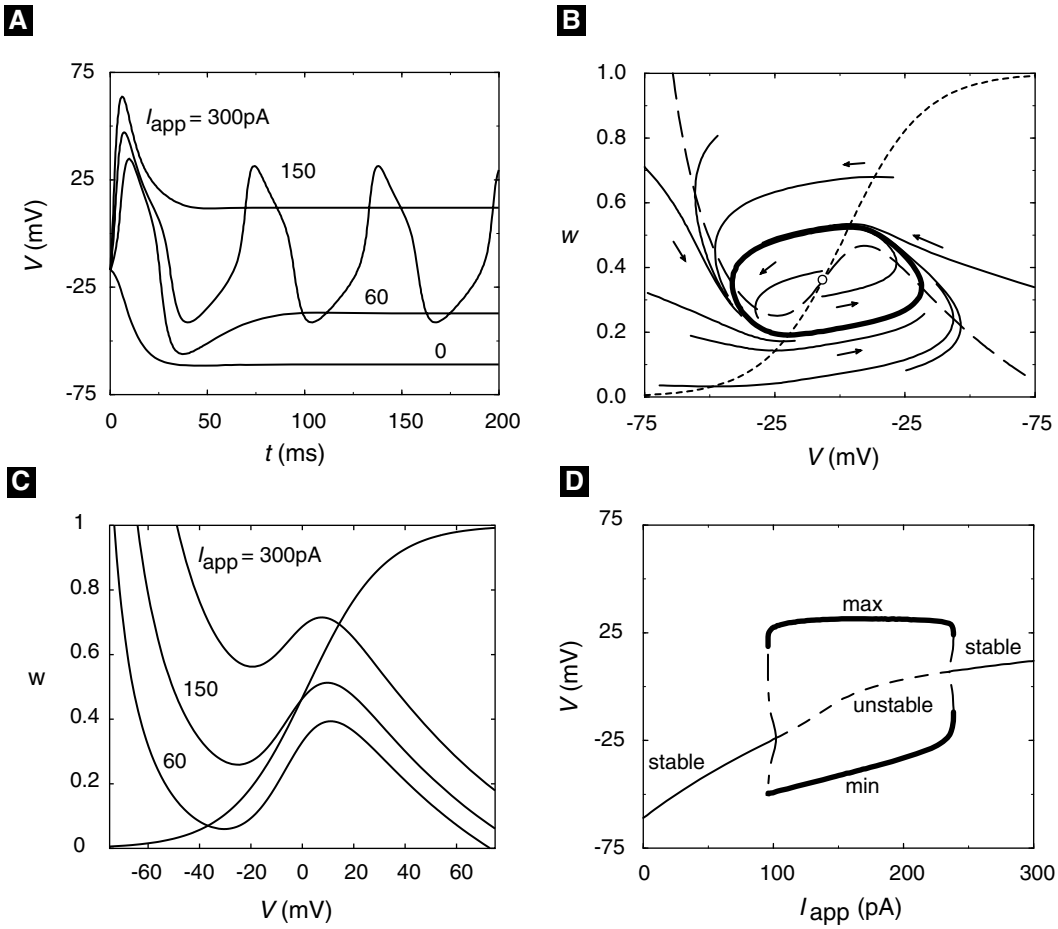

Figure 2.9 (A) Voltage simulation for the Morris–Lecar equations using the indicated applied currents and parameters as in Table 2.4. Oscillations occur at $I_{app} = 150$ pA. (B) The phase plane for the Morris-Lecar model for $I_{app} = 150$ pA. The heavy line is the limit cycle corresponding to the oscillation in (A), and the lighter lines are short trajectories that circulate in the counter–clockwise direction toward the stable limit cycle. The short arrows indicate the vector field. The V-nullcline is the long-dashed line and the w-nullcline is the short-dashed line. (C) Nullclines for several values of I_{app}. (D) A bifurcation diagram that catalogues the dynamical states of the Morris–Lecar model as a function of I_{app} with the other parameters fixed. The maximum and minimum of V on the limit cycle are represented by the heavy lines. Compare the values for $I_{app} = 150$ pA (long-dashed line) with the voltage record in (A).

Phase plane analysis plots for the Morris–Lecar model are shown in Figure 2.9B and Figure 2.9C. Figure 2.9B shows trajectories, nullclines, and the vector field for $I_{app} = 150$ pA, which leads to the pattern of repetitive spiking. The phase portrait consists of a number of representative trajectories together with a unique, closed trajectory indicated by the heavy line. This trajectory is called a *stable limit cycle* because it is

the cyclic curve to which all the neighboring trajectories converge no matter where in phase space they originate. The trajectories circulate around the steady state in a counterclockwise direction as indicated by the velocity vector field, which is shown as small arrows.

The nullclines are indicated by the lighter segmented lines. The V-nullcline, which has the inverted "N" shape, is given by the long-dashed line. It is the solution to

$$0 = -g_{Ca} m_\infty (V - V_{Ca}) - g_K w (V - V_K) - g_L (V - V_L) + I_{app} \tag{2.36}$$

for each value of w.

The w-nullcline is the solution to

$$0 = \frac{\phi(w_\infty - w)}{\tau} \tag{2.37}$$

for each value of V.

Note that the limit cycle in Figure 2.9B circulates around the intersection of the two nullclines. We saw in Figure 2.9A that different values of I_{app} lead to different behaviors and that $I_{app} = 150$ pA was the only value of the four tested that results in oscillations. Figure 2.9C shows how changing the value of I_{app} affects the nullclines of the system. We see that increasing I_{app} from 60 pA to 150 pA and then to 300 pA raises the V nullcline but leaves the w nullcline unaltered. If we examine Figure 2.9A and Figure 2.9C carefully, we notice something interesting: As we saw above, the limit cycle obtained when $I_{app} = 150$ pA circulates around the intersection of the nullclines at that parameter value. At $I_{app} = 300$ pA the system evolves to a steady state that corresponds to the intersection of the nullclines obtained for that I_{app}. The same is true for $I_{app} = 60$ pA. We know that a point on a nullcline corresponds to a point at which the variable of interest is not changing, and so it makes sense that the intersection of nullclines represents a combination of variables for which the system as a whole does not change. The intersection of the nullclines for $I_{app} = 60$ pA and $I_{app} = 300$ pA are examples of *fixed points*, and represent *stable steady states*. What is different about the intersection of nullclines obtained when $I_{app} = 150$ pA?

2.4.2 Stability Analysis

Fixed points can be either stable or unstable and the intersection of nullclines obtained when $I_{app} = 150$ pA is an unstable fixed point. Notice that the two trajectories that start nearest to the intersection of the nullclines in Figure 2.9B diverge away from the intersection and toward the limit cycle. The trajectory of the system is thus driven away from the intersection of the nullclines while at the same time being constrained to orbit around it. The existence of a stable limit cycle should be no more surprising than the existence of stable steady states. It corresponds to a closed trajectory to which all neighboring trajectories converge. The tools provided for phase plane analysis and stability analysis in some ODE packages make it easy to determine steady states, limit cycles, and stability, and therefore how a system like the Morris–Lecar model will behave.

Appendix A reviews how the *eigenvalues* determine the global stability properties of a linear system. Eigenvalues describe the solution of the linear system: Negative real eigenvalues indicate a stable solution, positive real eigenvalues indicate an unstable solution, and complex eigenvalues indicate the presence of oscillations in the solution. Stability analysis for nonlinear systems is not quite so straightforward, in that we can only determine the stability in such a system in a very small region around the a fixed point. In essence we linearize the system, either analytically (with a *Taylor series* as described in Appendix A) or numerically (with a software package). We then use the same tools that we used for the linear system in the small linearized region around the fixed point in the nonlinear system.

This book emphasizes the use of computational tools rather than mathematical analysis. An intuitive understanding of the concept of stability can be obtained without mathematical rigor. However, it must be stressed that there are myriad subtleties that can be appreciated only with an understanding of the underlying mathematics. The topic of stability analysis of linear and nonlinear equations is covered in more depth in Appendix A, and the student should be familiar with the analytical techniques discussed there in order to appreciate the output of computational tools. Other excellent sources covering this material on a reasonably introductory level are available (Edelstein-Keshet 1988; Kaplan and Glass 1995), and a particularly detailed analysis of the firing proterties of the Morris–Lecar system has been published (Rinzel and Ermentrout 1998).

The simulations in Figure 2.9A show that a stable limit cycle occurs for the Morris–Lecar model only for certain values of I_{app}, such as $I_{\text{app}} = 150$ pA. We can determine the stability of the fixed points corresponding to different values of I_{app} using a numerical package. The intersection of the nullclines for $I_{\text{app}} = 150$ pA indicated by the open circle in Figure 2.9B is an unstable steady state at $V = -.460$ and $w = 0.459$, a fixed point with eigenvalues $\lambda_{\pm} = 0.264$ and 0.033 (values are rounded). It is unstable because the eigenvalues are positive real numbers, and yet these parameters result in stable oscillations. This is an excellent example of how the local stability of a fixed point does not tell the whole story for a nonlinear system. Unlike the case with linear systems (covered in Appendix A), here positive eigenvalues can be associated with stable oscillations in phase space around the unstable fixed point.

Table 2.5 Fixed Points and Their Eigenvalues

I_{app}	V	w	Eigenvalue	Eigenvalue
0 pA	−60.855 V	0.015	−0.037	−0.096
60 pA	−37.755 V	0.070	$-0.055 + i0.063$	$-0.055 - i0.063$
110 pA	−19.219 V	0.196	$0.055 + i0.045$	$0.055 - i0.045$
150 pA	−0.460 V	0.459	0.264	0.033
180 pA	6.656 V	0.577	$0.025 + i0.139$	$0.025 - i0.139$
300 pA	14.302 V	0.694	$-0.137 + i0.117$	$-0.137 - i0.117$

Using a systematic stepping procedure, we can test the stability of the system over a wide range of parameter values. Table 2.5 shows the eigenvalues for the values of I_{app} that we have examined plus some additional intermediate values. As I_{app} is increased from $I_{app} = 0$, the eigenvalues are seen to change from negative (stable node) to complex with negative real parts (stable focus), to complex with positive real parts (unstable focus) as oscillations emerge. The oscillations at $I_{app} = 150$ correspond to eigenvalues that are both real and positive (unstable node). As I_{app} is increased further, the eigenvalues become complex again with positive real parts, and eventually become complex with negative real parts as oscillations cease. Fixed points at which the qualitative character of the solution changes with a change in a parameter are called *bifurcation* points. The mathematical properties of bifurcations are also treated in more detail in Appendix A. In particular, Appendix A discusses the *Hopf bifurcation theorem*, which establishes the conditions that result in the limit cycle oscillations that we see here.

By making even smaller changes in I_{app} and testing the stability of the steady state, it is possible to locate the specific values at which the stability of the steady state changes. This procedure could become very laborious, and so numerical algorithms have been developed that allow investigation of bifurcations to be done automatically. In the bifurcation diagram shown in Figure 2.9D, the characteristic values of the membrane potential are plotted on the ordinate as a function of I_{app}. The thin full and dashed lines are the steady–state values of V for each value of I_{app}, with the full lines representing stable steady states and the dashed lines unstable states. The points $I_{app} \approx 94$ pA and 212 pA are bifurcation points where the stability of the steady state changes. Near these points two new dynamical features appear: a stable limit cycle and an unstable limit cycle. This type of bifurcation is called a *subcritical Hopf bifurcation*, as discussed in Appendix A. Note that while the detail is not apparent in Figure 2.9D, the unstable limit cycle turns back and then coalesces at a turning point bifurcation with the stable limit cycle at a value of I_{app} that is smaller than the bifurcation point, and therefore there is a small region of bistability. The bifurcation diagram in Figure 2.9D also records the maximum and minimum values of V on the limit cycles with heavy full lines. For example, at $I_{app} = 150$ pA the points on the heavy line correspond to the maximum and minimum of the spikes in Figure 2.9A.

2.4.3 Why Do Oscillations Occur?

If the following three conditions on the Morris–Lecar equations hold, then oscillations will occur:

- the V nullcline has the inverted "N" shape like that in Figure 2.9B;
- a single intersection of the V- and w-nullclines occurs between the maximum and minimum of the "N;"
- the rate of change of V is much greater than w.

All three conditions are met for the parameter values in Table 2.4, giving rise to oscillations in Figure 2.9A. The importance of the slow change in w, i.e., the "delay" of

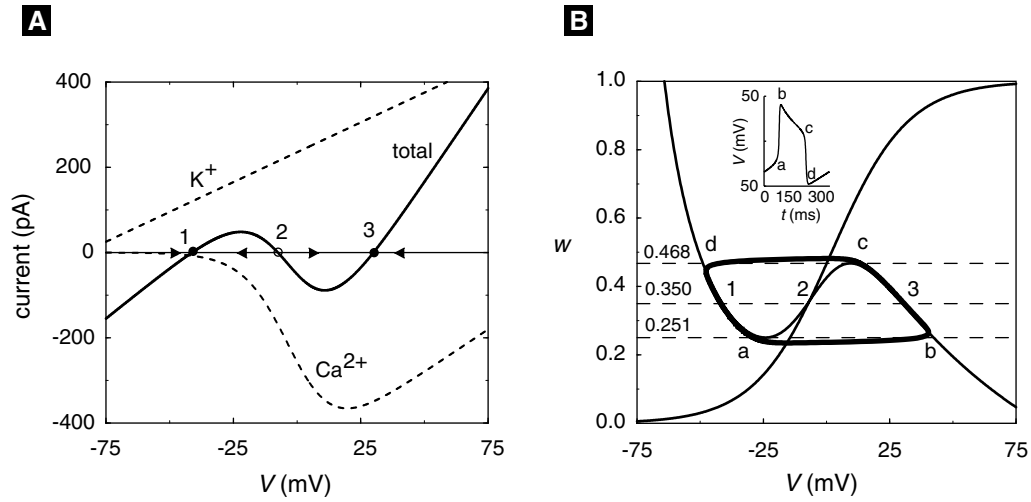

Figure 2.10 (A) The K^+, Ca^{2+}, and total current ($I_{Ca} + I_K + I_{leak} - I_{app}$) when $w = 0.35$. States 1 and 3 are stable steady states, and state 2 is unstable as indicated by the velocity vectors. (B) The phase plane for the Morris–Lecar model for $I_{app} = 150$ pA, except that $\tau(V)$ has been increased by a factor of ten. The values $w = 0.468$ and 0.251 correspond to the maximum and minimum of the V-nullcline. The points 1, 2, and 3 at $w = 0.350$ are the steady states in (A). Inset shows the voltage record for a single spike.

the delayed rectifier, can be seen by examining the trajectories in Figure 2.9B. If the rate of change of w were large with respect to V, then the trajectories would not depolarize and hyperpolarize rapidly as they do in Figure 2.9A. This is tested by decreasing the value of the parameter ϕ, thereby increasing the value of the characteristic time for relaxation of w.

By altering the time scale we see why oscillations occur when the rate of change of V is very much faster than w and the nullclines have the shape in Figure 2.9. In this case, we can treat changes in V under the assumption that w is constant, and we need only to consider the voltage equation with w fixed:

$$C\frac{dV}{dt} = -g_{Ca}m_\infty(V - V_{Ca}) - g_K w(V - V_K) - g_L(V - V_L) + I_{app}. \tag{2.38}$$

Because only the voltage is changing on this time scale, we can examine its dynamical behavior using the one–dimensional phase portrait, rather than a phase plane. This is shown in Figure 2.10A, where the total current, which is proportional to the rate of change of V, is plotted along with the Ca^{2+} and K^+ currents for $w = 0.35$ and $I_{app} = 150$ pA. The total current vanishes at three points, which are the steady states for the voltage when w is fixed. States 1 and 3 are stable, and state 2 is unstable, as indicated by the velocity vectors in the figure. Note that at state 1 the membrane is polarized and the outward K^+ current dominates the Ca^{2+} inward current, whereas the opposite holds true at state 3. As we shall see, the oscillations can be thought of as transitions back

and forth between the polarized and depolarized states, driven by slow changes in activation of the delayed rectifier current.

Figure 2.10A also explains why the V-nullcline in the Morris–Lecar model has the inverted "N" shape: The K^+ and leak currents exceed the inward Ca^{2+} current at polarized voltages between states 1 and 2, whereas the Ca^{2+} current exceeds the other currents between states 2 and 3. This voltage-dependent competition between inward and outward currents leads to a maximum and minimum in total current and therefore the inverted "N" shape for the nullcline.

The three steady states of the voltage also can be found graphically in the phase plane of Figure 2.10B by locating the intersection of the line $w = 0.35$ with the V-nullcline. It is clear from the figure that if w exceeds 0.468 (the maximum on the right branch of the V-nullcline), then the voltage has only a single polarized steady state (intersection with w) on the far left branch of the V-nullcline. Similarly, if w is smaller than 0.251 (the minimum on the left branch of the V-nullcline), then the voltage has only a single depolarized steady state on the right branch. For $0.251 \leq w \leq 0.468$ two stable steady states and one unstable state occur, and the voltage is said to be *bistable*.

To understand how bistability on the fast time scale (neglecting w) leads to oscillations in the complete system, we need to understand how w changes on the longer time scale. Assume that initially, the membrane is polarized at state 1 in Figure 2.10B, with $w = 0.35$. Because $w = 0.35$ is above the w-nullcline at point 1, w will decrease. As w decreases, V will stay close to the V-nullcline because it relaxes rapidly to the closest steady–state value. The trajectory thus follows the polarized branch, as indicated by the heavy line, until the minimum at $w = 0.251$ is reached. Beyond the minimum (near a), stable polarized states no longer exist, and V rapidly relaxes to the only remaining steady state (near b), which is on the depolarized, far right branch of the V-nullcline. During the depolarization, however, the w-nullcline is crossed. Thus on the depolarized branch, w increases and tracks the V-nullcline upward until the maximum at $w = 0.468$ is reached (near c) and the membrane rapidly repolarizes to the polarized branch (near d).

The abrupt transitions from the polarized to depolarized branch and back again have led to the name *relaxation oscillator* for systems of equations that have well-separated time scales. For the parameters in Figure 2.9, the Morris–Lecar model is not a relaxation oscillator. However, when the characteristic time for w is increased by a factor of 10 (by decreasing ϕ), the limit cycle (heavy line in Figure 2.10B) closely approximates that for a relaxation oscillator. If the characteristic time were increased sufficiently, or the characteristic time for V were decreased sufficiently by altering the capacitance, then the trajectory would coincide with the bistable portions of the V-nullclines, and the rapid excursions of the voltage would occur precisely at $w = 0.251$ and 0.468. The inset in Figure 2.10B shows a single voltage spike that illustrates the rapid upstroke and downstroke for the limit cycle. The inset also illustrates that the shape of the depolarized and polarized portions of the spike reflects the shape of the two branches of the V-nullcline.

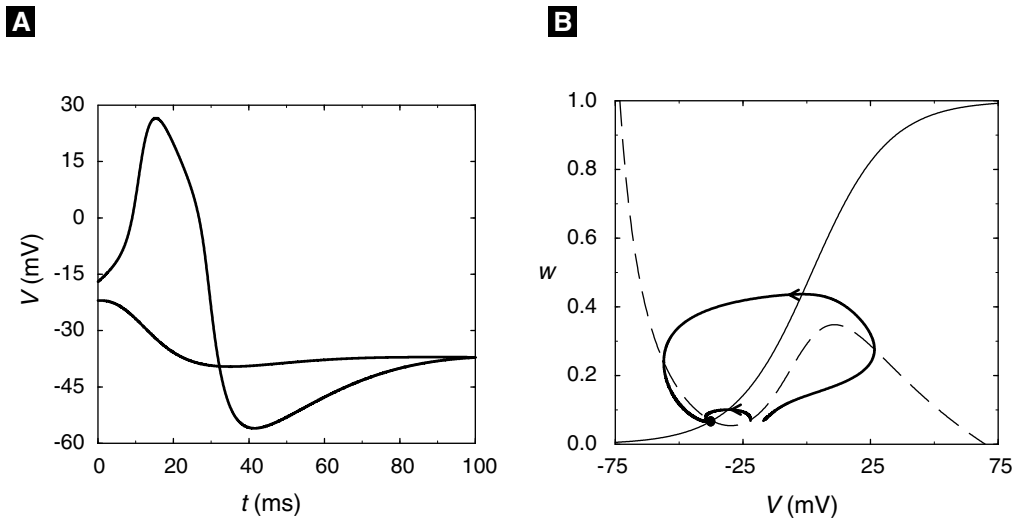

Figure 2.11 Excitability in the Morris–Lecar model for $I_{app} = 60$ pA. (A) An initial deviation of the voltage to -22 mV relaxes rapidly to the steady–state voltage, whereas a deviation to -17 mV produces an action potential. (B) The trajectories in (A) represented in the phase plane. When V changes much faster than w, the location of the V-nullcline (long-dashed line) sets the threshold for action potential spikes.

2.4.4 Excitability and Action Potentials

Another dynamical feature of the Morris–Lecar model is *excitability*. A useful working definition of excitability is that a system is excitable when small perturbations return to the steady state, but larger (i.e., above a threshold) perturbations cause large transient deviations away from the steady state. An example of this is shown in Figure 2.11A, where the time course of the voltage with an applied current of 60 pA and initial conditions of $w(0) = w^{ss} = 0.070$ and either $V(0) = -22$ or -17 mV are used. For subthreshold $V(0)$ such as -22 mV, the voltage increases only slightly before it decreases monotonically to its steady state–value of about -37 mV. For suprathreshold deviations, like that for $V(0) = -17$ mV, the voltage increases dramatically, producing an action potential spike before returning to steady–state.

The explanation for excitability can be understood most easily in the phase plane. In Figure 2.11B we have plotted the trajectories for the two initial conditions in Figure 2.11A along with the two nullclines. The trajectories for subthreshold initial conditions like $V(0) \leq -22$ mV start at points in phase space *above* the V-nullcline and *below* the w nullcline. This implies that the initial velocity vector, and therefore the initial trajectory, points in the direction of smaller potentials and larger values of the activation of the delayed rectifier K^+ current. Thus the voltage begins to decrease and continues to do so because the K^+ current activates as w increases. This contrasts with the trajectory that starts at $V(0) = -17$ mV, for which the initial velocity vector points in the direction of

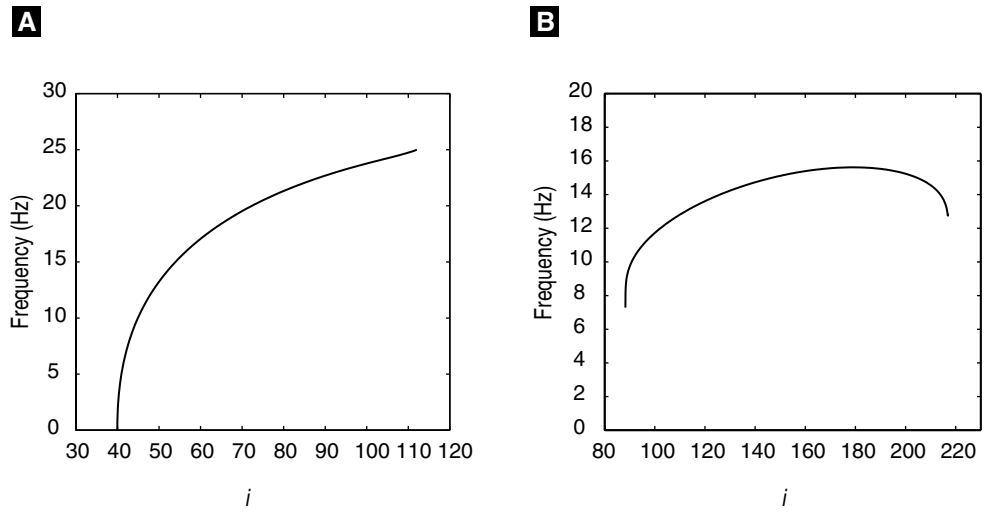

Figure 2.12 Examples of voltage–freqency plots for the Morris–Lecar model with parameters that result in (A) Type I dynamics and (B) Type II dynamics. Note that the axes are somewhat different. Plotted according to Rinzel and Ermentrout (1998).

increasing voltage. Even though w is increasing in this region, which is also below the w-nullcline, the rate of increase of voltage exceeds that of w, and the trajectory moves to higher voltages until it crosses the V-nullcline and begins to decrease.

The threshold value of $V(0)$ above which action potentials occur depends on the shape of the nullclines and the rate of activation of w (altered by ϕ). However, it is close to the point where a line drawn parallel to the V axis at w^{ss} crosses the V-nullcline. It is not hard to check that it will approach this point as w is made to change more slowly than V.

2.4.5 Type I and Type II Spiking

Many investigators are now interested in applying biophysical models of neurons and other spike–generating mechanisms to the study of information transfer using information–theoretic measures. It is particularly important, therefore, that the dynamical behavior of a model be characterized over the space of parameters and that the characteristics of the spike generating model match the intended use. Both the Hodgkin–Huxley model, described below, and the Morris–Lecar model produce trains of action potentials with commonly used parameter sets and when sufficiently depolarized. Muscle fiber and axons innervating muscle fiber are examples of situations where a strong, consistent signal is required. In our investigations of the Morris–Lecar model, we have seen that depolarization beyond threshold results in oscillations that begin at a characteristic nonzero frequency. This behavior has been defined as a Type II oscillator (Rinzel and Ermentrout 1998).

Many neurons exhibit firing properties that are fundamentally different from those of the Type II oscillator. Models of these cells can produce arbitrarily low frequencies of oscillations. These models are classified as Type I oscillators (Rinzel and Ermentrout 1998). The Morris–Lecar model can exhibit Type I or Type II behavior, depending on the parameters that are chosen, and the Hodgkin–Huxley model also can be modified to show this behavior. See Table 2.6 for the Morris–Lecar Type I parameters that differ from Type II parameters. Examples of voltage–frequency plots for the Morris–Lecar model in these two regimes are shown in Figure 2.12. The Morris–Lecar Type II oscillator might not be appropriate for the study of subtle aspects of information transfer or intra–neuronal coupling. We have seen that Type II spiking results from a subcritical Hopf bifurcation as input current is increased. Type I spiking results from a saddle-node bifurcation. The difference between these two bifurcations is discussed in Appendix A. We also note that there are other levels of complexity for spiking and oscillating models. Models of bursting cells, which exhibit trains of oscillations separated by periods of quiescence, require additional slow variables. These models will be discussed in detail in Chapter 5.

2.5 The Hodgkin–Huxley Model

Ordinarily, a discussion of membrane electrophysiology might begin with the famous model of the squid giant axon developed by Hodgkin and Huxley (the HH model) (Hodgkin and Huxley 1952). Our goal here has been to facilitate a clear mathematical understanding of oscillatory behavior in systems of ion channels. While it remains a seminal accomplishment in the history of physiology, the HH model is complicated and not amenable to the phase plane methods of analysis that we have used to understand dynamical electrical behavior in cells. The student should be familiar with the HH model, for historical reasons and because it is still widely used. We cannot cover the work of Hodgkin and Huxley in the detail it deserves, but the concepts learned in the study of the Morris–Lecar oscillator will aid the student in understanding the HH model. We recommend that the student consult Bertil Hille's *Ionic Channels of Excitable Membranes* (Hille 2001), which contains one of the best treatments of the HH model and the history behind it. "Hille" is also the best consolidated source of information

Table 2.6 Morris–Lecar Type I Oscillator Parameters

Parameter	Value
g_{Ca}	4 mS/cm^2
$v3$	12 mV
$v4$	17.4 mV
ϕ	0.066/ms

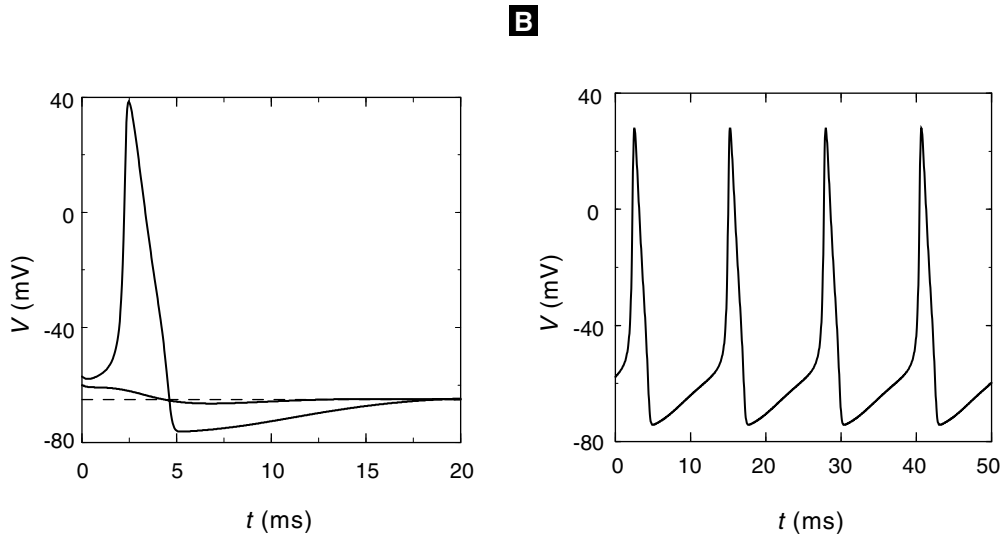

Figure 2.13 (A) The solution of the Hodgkin-Huxley equations for three different initial values of the membrane potential and no applied current. When the initial value exceeds ca. −59 mV, an action potential is produced. (B) Continuous spiking occurs under the same conditions with an applied current $I_{\text{app}} = 15$.

about the biophysics of ion channels, and it should be familiar to any person attempting to model electrical behavior.

The HH model is empirical (Hodgkin and Huxley 1952). Many voltage clamp experiments were performed by Hodgkin and Huxley, and their data were fit to expressions that they incorporated into the model without consideration of an underlying mechanism for the channel gates. One of the remarkable aspects of Hodgkin and Huxley's work is that their model was developed without a molecular understanding of the mechanism. In fact, it required almost thirty years of intensive research after their work to formulate a realistic cartoon of the mechanisms underlying the ionic currents in cells. Although Hodgkin and Huxley justified these expressions on empirical grounds, it is possible to derive the gating expression used in the Hodgkin–Huxley model using mechanistic models.

From their voltage clamp and other measurements, Hodgkin and Huxley deduced that the sodium conductance involved two voltage-dependent "gates," an *activation* gate and an *inactivation*, gate and that the potassium conductance had a single activation gate. Note that the presence of an inactivation gate differs from the Morris–Lecar model. To account for these facts they represented the ionic conductances in the following form:

$$g_{\text{Na}} = \bar{g}_{\text{Na}} m^3 h, \tag{2.39}$$

$$g_{\text{K}} = \bar{g}_{\text{K}} n^4, \tag{2.40}$$

where the terms $\bar{g}$ represent maximal conductances, and m and n are the activation gating variables and h the inactivation. The exponents on m and n were chosen for the best fit to experimental data. These gating variables were postulated to satisfy linear differential equations where the variables "relax" to voltage–dependent values, e.g., m_∞, that vary between zero and one with voltage-dependent time constants, e.g., τ_m.

Putting the ODEs for the gating variables together with (2.11) gives the primary equations for the Hodgkin–Huxley model:

$$\begin{aligned} CdV/dt &= -\bar{g}_{\mathrm{Na}} m^3 h(V - V_{\mathrm{Na}}) - \bar{g}_{\mathrm{K}} n^4 (V - V_{\mathrm{K}}), \\ &\quad - \bar{g}_{\mathrm{leak}}(V - V_{\mathrm{leak}}) + I_{\mathrm{app}}, \end{aligned} \tag{2.41}$$

$$dm/dt = -(m - m_\infty)/\tau_m, \tag{2.42}$$

$$dh/dt = -(h - h_\infty)/\tau_h, \tag{2.43}$$

$$dn/dt = -(n - n_\infty)/\tau_n. \tag{2.44}$$

Hodgkin and Huxley added the third conductance $\bar{g}_{\mathrm{leak}}$ to their voltage equation to account for a small voltage-independent conductance that they attributed to a "leak" in the membrane, possibly through their microelectrode. The nonlinear terms in (2.41) are obvious in the activation and inactivation gates. Not so obvious are the nonlinearities in (2.42)–(2.44). However, all the voltage-dependent terms in those equations are nonlinear functions of V as well.

The student should solve the HH equations to provide a basis for comparison and further exploration (Exercise 9b). The equations for the Hodgkin–Huxley spike generator are readily available from other sources, and it is not difficult to run simulations with a package for solving ODEs. One must be careful to choose a suitable numerical method of solution due to the nonlinear equations. Figure 2.13 shows several simulations that can be made with the HH equations. The *Runge–Kutta* method has been used with a time step of 0.05, which is appropriate because reducing the time step to 0.01 gives no noticeable change in the results.

Figure 2.13A shows calculations with $I_{\mathrm{app}} = 0$, but with $V(0) = -65$, -60, and -57 mV. The steady state for the voltage with these parameters is clearly -65 mV; however, if the initial value of V exceeds about -59 mV, then the equations produce an action potential spike, and we have another example of a Type II oscillator. The Hodgkin-Huxley equations can also produce repetitive firing of action potentials. This is illustrated in Figure 2.13B. The parameters in that simulation are identical to those in Figure 2.13A, except that $I_{\mathrm{app}} = 15$.

2.6 FitzHugh–Nagumo Class Models

We have seen that a fast variable with a cubic nullcline for voltage and a slower variable with a monotonically increasing nullcline for channel opening are sufficient to produce oscillations. In some cases, and particularly for mathematical analysis, it may be beneficial to completely abstract the mathematical equations for an oscillator from

the underlying physical processes in order to understand general properties of these systems. Because two–variable systems are useful for the phase plane methods we have discussed, we can contrive such a system.

The two differential equations will be functions of both state variables:

$$\begin{aligned}\frac{dv}{dt} &= f(v,w),\\ \frac{dw}{dt} &= g(v,w).\end{aligned} \tag{2.45}$$

By definition, the nullcline is obtained by setting the right–hand side of the equation to zero and plotting the function in the (v,w) phase plane. We can create the behavior we desire by specifying the shapes of $f(v,w)$ and $g(v,w)$. The slow variable, w, is easiest, because we want $g(v,w)$ to be similar to a line describing the increase of v with w. Note that v here is the dependent variable for the equation for a line:

$$g(v,w) : v = \gamma w, \tag{2.46}$$

and therefore

$$\frac{dw}{dt} = v - \gamma w \tag{2.47}$$

where γ is the slope parameter.

The fast variable v will have a form similar to (2.47) with w as the dependent variable:

$$f(v,w) : w = f(v), \tag{2.48}$$

and therefore

$$\frac{dv}{dt} = f(v) - w. \tag{2.49}$$

Because we know that w needs to be a cubic function of v, let us try

$$f(v) = Bv(v-\beta)(\delta - v), \tag{2.50}$$

where A is a parameter to scale the amplitude of the curve. The equations for the complete system are therefore

$$\begin{aligned}\frac{dv}{dt} &= Av(v-\beta)(\delta - v) - Cw,\\ \frac{dw}{dt} &= \epsilon(v - \gamma w).\end{aligned} \tag{2.51}$$

The parameter ϵ has been added to more easily control the speed of one variable relative to the other, and the parameter C affects the coupling strength. For an appropriate choice of all of the parameters, we would expect that this system of abstracted differential equations would produce oscillations (Exercise 10b).

This dynamical paradigm appeared first in cellular neuroscience in simplifications of the Hodgkin–Huxley equations by FitzHugh (1961), and later as part of an independent development by Nagumo et al. (1962). In fact, the various parameters we have contrived have physical interpretations in the context of a simplification of the Hodgkin–Huxley circuit diagram we discussed earlier. This type of system, involving a linear nullcline for the slow variable and a cubic nullcline that has the inverted "N" shape for the fast variable, are given the generic name *FitzHugh–Nagumo* (or FH-N) models. The FH-N model is discussed in more detail in Section 7.5.2 and in Appendix B.

2.7 Summary

Voltage gated ion channels and the currents that flow through them underlie much of the electrical behavior of cells. We derived a mechanism–based model for ion channels and found that we could produce oscillatory behavior in electrical membranes with only two variables. Therefore, we could analyze the underlying dynamics with phase plane techniques and other methods of dynamical systems analysis. The dynamical features of "slow" variables coupled to "fast" variables with either "N"-shaped or inverted "N"-shaped nullclines are characteristic of FitzHugh–Nagumo type oscillators common to many biological mechanisms at the cellular level. In addition to producing oscillations in the barnacle muscle, the same dynamical structures will appear in mechanistic models of insulin secretion (Chapter 4) and Ca^{2+} oscillations (Chapter 5).

Suggestions for Further Reading

Because of the introductory nature of this material, there are several excellent books to serve as resources for further study and a different perspective:

- *Principles of Neural Science*, edited by Eric Kandel, James Schwartz, and Thomas Jessel, and *Fundamental Neuroscience*, edited by Michael Zigmond, Floyd Bloom, Story Landis, James Roberts, and Larry Squire. These are general introductory textbooks on neuroscience, including chapters on ion channels and electrical behavior (Kandel et al. 2000; Zigmond et al. 1999).
- *Ionic Channels of Excitable Membranes*, Bertil Hille. As discussed in the text above, this is the "bible" of ion channels, with a particularly complete treatment of the Hodgkin–Huxley axon model and the work behind it by those and other scientists (Hille 2001).
- *Cellular Biophysics*, Volume 2, Thomas Weiss. Volume two of this two–volume set is a more expanded discussion of the electrical properties of cells, and also contains a chapter on the Hodgkin–Huxley model (Weiss 1996).

- *Foundations of Cellular Neurophysiology*, Daniel Johnston and Samuel Wu. Covers the introductory material discussed here as well as advanced topics such as transmitter release, plasticity, elementary networks, and extracellular electrical behavior (Johnston and Wu 1995).
- *Methods in Neuronal Modeling*, Christof Koch and Idan Segev, editors. This is a compilation of chapters from various authors on a wide variety of topics related to neuronal modeling. Particularly relevant is the chapter by John Rinzel and Bard Ermentrout on the "Analysis of Neural Excitability and Oscillations," which describes phase plane methods in the context of the Morris–Lecar model (Koch and Segev 1998).
- *Mathematical Models in Biology*, Leah Edelstein-Keshet. This is a great introductory textbook on general mathematical biology. Chapter 8 contains material on the FH-N oscillator and a general treatment of oscillations and phase plane analysis (Edelstein-Keshet 1988).
- *Mathematical Physiology*, James Keener and James Sneyd. Keener and Sneyd treat the topics presented in this chapter, as well as many other topics in physiology, from a more analytic perspective as opposed to the computational focus presented here (Keener and Sneyd 1998).

2.8 EXERCISES

1. The following problems explore calclulation of the Nernst potential and the resting membrane potential.

   (a) Fill in the missing values in the following table:

Ion	Cytoplasmic Concentration (mM)	Extracellular Concentration (mM)	Equilibrium Potential (mV)
K^+	400	20	
Na^+	50	440	
Cl^-	40	560	

   (b) Calculate the resting membrane potential given the following conductances:

$$g_{Na} = 0.5 \cdot 10^{-6} \text{ S},$$
$$g_K = 10 \cdot 10^{-6} \text{ S},$$
$$g_{Cl} = 2.5 \cdot 10^{-6} \text{ S}.$$

   (c) Fill in the missing information in the following table:

Conductance Change	Ion Action	Membrane Potential Change
large g_K increase		
	Na^+ enters	
		V moves to V_{Cl}

2. Assume that a proto-cell has a membrane capacitance of 1 μF/cm^2 and contains only K^+ selective channels. The initial intracellular and extracellular concentrations for K^+ are given in the table above, and there are intracellular and extracellular anions A^- equal in concentration to K^+.

(a) If the membrane K^+ channels are opened, what is the steady–state voltage across the membrane assuming that ion concentrations do not change?

(b) How many K^+ ions must move out of the cell per cm^2 to achieve a voltage difference equal to that in part (a)?

(c) Assuming that our proto-cell is perfectly round and that the extracellular K^+ concentration does not change, plot the final intracellular K^+ concentration as a function of the diameter of the cell. Use a range of realistic diameter values and the number of ions transfered that you calculated in part (b).

(d) Assuming that the extracellular K^+ concentration remains constant, what would the reversal potential be for the range of intracellular K^+ concentrations calculated in part (c).

(e) How do you reconcile parts (a) and (d)?

3. Derive (2.5) from (2.8). *Hint:* assume steady state and $I_{\text{app}} = 0$.

4. Verify the steps between (2.16) and (2.22).

5. Use the results in Exercise 4 to verify that the expressions in (2.23)–(2.24) are correct. Show that a special case of (2.24) when $\alpha = -\beta$ is

$$\tau = \frac{1}{2\sqrt{k_o^+ k_o^-}\cosh((V - V_o)/2S_o)}. \tag{2.52}$$

[*Hint*: Recall that $\tanh(x) = (e^x - e^{-x})/(e^x + e^{-x})$ and $\cosh(x) = (e^x + e^{-x})/2$.]

6. It is possible to estimate a characteristic time for the relaxation of the membrane potential using (2.27). When the channels are completely open, show that the equation can be written

$$dV/dt = -(V - V_{\text{rev}})/\hat{\tau} + I_{\text{app}}/C, \tag{2.53}$$

where $\hat{\tau} = C/\bar{g}$. Show that $\hat{\tau}$ is the characteristic time for relaxation of the voltage to a steady–state value $V^{\text{ss}} = V_{\text{rev}} + I_{\text{app}}/\bar{g}$.

7. For biological membranes a typical capacitance per unit area is 1 μF/cm^2, whereas conductances per unit area are in the range 10^{-4} to 10^{-3} S/cm^2. Using these estimates, show that typical relaxation times for the membrane potential are in the range of 1 to 10 ms.

8. Write a program suitable for simulating the Morris–Lecar equations (2.30)–(2.34) for the parameter values given in Table 2.4 and the initial conditions $V(0) = -60$ and $w(0) = 0.01$.

(a) Use the program to solve the Morris–Lecar model for the four values of I_{app} given in Figure 2.9A.

(b) Plot the nullclines and simulate this model in the phase plane to verify that there is a unique stable limit cycle. Locate the steady states and calculate the eigenvalues for representative values of I_{app}.

(c) Show that the time constant of the delayed rectifier in the Morris–Lecar model determines whether or not the steady state at $I_{\text{app}} = 150$ pA is stable or unstable and also determines the maximum and minimum values of the voltage on the limit cycle.

(d) For $I_{\text{app}} = 60$ pA check that the value of $V(0)$ above which action potentials occur is close to the point where a line drawn parallel to the V axis at w^{ss} crosses the V-nullcline. Also verify that it will be exactly at that point in the limit that w changes

much more slowly than the voltage. [Hint: Increasing the parameter ϕ increases the time constant for w.]

(e) Explain how you could locate the unstable limit cycles near the bifurcation point in the Morris–Lecar model in Figure 2.9 by integrating the equations *backwards* in time. Use a plot to demonstrate this.

9. Exploration of the Hodgkin–Huxley equations.

(a) Read Chapter 2 of Hille's *Ionic Channels of Excitable Membranes* (Hille 2001). Write a paragraph explaining in words how the HH model works, and include an explanatory diagram.

(b) Research the voltage–dependent expressions for time constants and the asymptotic limits in (2.42)–(2.44), together with parameters. Replicate Figure 2.13. [*Hint*: See Hodgkin and Huxley (1952) or another source such as Keener and Sneyd (1998).]

10. System (2.51) constitutes a FitzHugh–Nagumo model. Select parameters for these equations that are likely to result in oscillatory behavior.

(a) Sketch or calculate the nullclines.

(b) Add a parameter to apply external current, and simulate action potentials by solving the equations in time.